arXiv:2201.07591v2 [cs.NI] 23 Mar 2022

RIS-Aware Indoor Network Planning: The Rennes Railway Station Case

Antonio Albanese[1,2], Guillermo Encinas-Lago[1], Vincenzo Sciancalepore[1], Xavier Costa-Pérez[3,1], Dinh-Thuy Phan-Huy[4], Stéphane Ros[5]
[1]NEC Laboratories Europe, 69115 Heidelberg, Germany
[2]Departamento de Ingeniería Telemática, University Carlos III of Madrid, 28911 Leganés, Spain
[3]i2cat Foundation and ICREA, 08034 Barcelona, Spain
[4] Radio InnOvation (RIO) Department, Orange Innovation (INNOV), 92320 Chatillon, France
[5]Société nationale des chemins de fer français, 93210 Saint-Denis, France

***Abstract*—Future generations of wireless networks will offer unrivalled performance via unprecedented solutions: *metasurfaces* will drive such revolution by enabling control over the surrounding propagation environment, always portrayed as a tamper-proof black box. The reconfigurable intelligent surface (RIS) technology, envisioned as the discrete version of a metasurface, can dynamically alter the propagation of the impinging signals by, e.g., steering the corresponding beams towards controllable directions. This will unlock new application opportunities and deliver advanced end-user services.**

However, this fascinating solution comes at non-negligible costs: RISs require ad-hoc design, deployment and management operations to be fully exploited. In this paper, we tackle the RISs placement problem from a theoretical viewpoint, showcasing a large-scale solution on synthetic topologies to improve communication performance while solving the *dead-zone* problem. Additionally, our mathematical framework is empirically validated in a realistic indoor scenario, the Rennes railway station, showing how a complex indoor propagation environment can be fully disciplined by an advanced RIS installation.

I. Introduction

Recently, the new generation of cellular networks has been successfully integrated and deployed bringing along new business opportunities. However, the revenue-hungry telco operators continuously look for innovative solutions to enable new use cases, which involve new players into the engaged business model. In this context, one emerging technology aims at undermining the classical communication paradigm—that dogmatized the radio propagation environment as an ungovernable box—providing new means to exploit the signal properties: *reconfigurable intelligent surfaces (RISs)* [1]–[4].

Agility and flexibility represent the added-value of this solution [5], [6]: while RISs can be dynamically and continuously configured, they draw little power with affordable installation and maintenance costs [7]. This makes such a technology the best candidate to solve the mobile dead-zone problem in indoor scenarios by enabling very dense RIS-based network deployment at low Capital Expenditure (CAPEX). For instance, as shown in Fig. 1, the existing network infrastructure in a real railway station may fail to guarantee satisfactory performance within the entire environment: *How to solve the dead-zone problem with a very limited investment?* Ad-hoc RISs design and deployment strategies might be the correct answer. Indeed, while RISs properly steer the incoming electromagnetic waves towards specific directions, interference is also focused onto unwanted areas, if not properly handled [8]. This issue exacerbates the overall deployment complexity calling for advanced optimization techniques to strike the optimal trade-off between RISs density and the corresponding spurious detrimental interference.

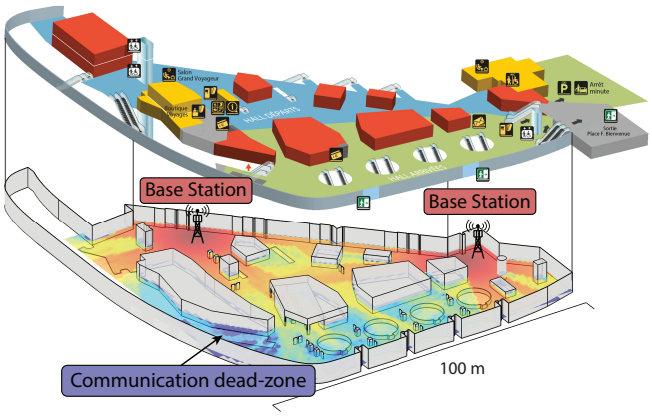


Fig. 1: Railway station topographic map and related power heatmap showing the dead-zone problem (Rennes, France).

Related work. In the literature, the generic base stations (BSs) deployment problem has been exhaustively investigated, e.g. in [9], [10]. The major drawback of such works lies in the isotropic antenna radiation assumption making the problem easy-to-solve via graph-coloring algorithms or convex programming approaches. When dealing with directive transmissions—e.g., millimeter waves (mmWaves) above 6 GHz—a new degree of freedom is introduced: the beam orientation. Specifically, mmWave BSs must be properly placed and electronically oriented to effectively beam towards specific locations leveraging on the available channel state information

This work was supported by EU H2020 RISE-6G (grant agreement 101017011) and EU H2020 METAWIRELESS (grant agreement 956256) projects. We thank Guillaume Grao for his support.
Email of corresponding author: antonio.albanese@neclab.eu

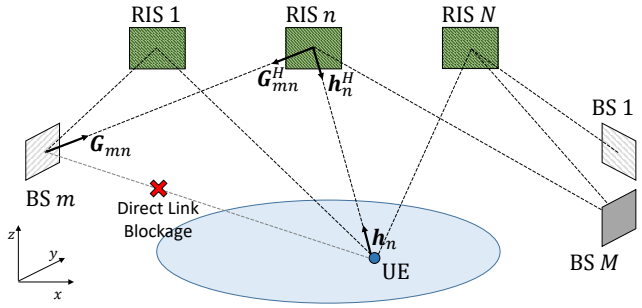


Fig. 2: Geometrical representation of the considered scenario including BSs, the RISs and one sample user equipment (UE).

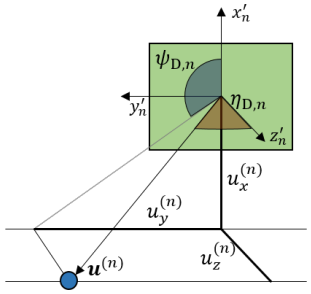


Fig. 3: Geometrical representation of one sample user equipment (UE) in the n-th RIS reference system.

(CSI) [11], [12]. Nonetheless, an optimal RISs deployment is even harder to achieve: on the one hand, RISs deployment requires prior information on the applied RISs configurations; on the other hand, RISs configurations can be obtained only upon fixing the BSs and RISs positions. To overcome this issue and make the analysis tractable, simplistic assumptions on agnostic RISs optimization can be done [13].

Contributions. Differently, our solution goes one step beyond and jointly tackles the optimal RISs placement and configuration problems without any unpractical assumption on the available CSI. We formulate the overall optimization framework and rely on the well-known Block Coordinate Ascent (BCA) [14] to devise RISA, a RIS-Aware network planning solution that iteratively derives the RISs configurations and optimally places the required number of RISs within the area. We i) develop a new lightweight ray-tracing model for multi-RIS scenarios, ii) analytically and empirically prove its short convergence time, iii) show its efficiency in large-scale scenarios and iv) demonstrate outstanding performance in a realistic indoor environment, namely the Rennes Train Station in France, to improve the existing cellular infrastructure of one of the major European operators and solve the dead-zone problem, as shown in Section VI.

Notation. We denote matrices and vectors in bold while each of their element is indicated in roman with a subscript. $(\cdot)^{\mathrm{T}}$ and $(\cdot)^{\mathrm{H}}$ stand for vector or matrix transposition and Hermitian transposition, respectively. The L2-norm of a vector is denoted by $\|\cdot\|$.

II. System Model

We consider the RIS-enabled wireless network depicted in Fig. 2, wherein N RISs are deployed to assist M BSs to extend their communication coverage in a given area of interest $\mathcal{A}$. We model each BS as a uniform linear array (ULA) with N_b antennas, and each RIS as a planar linear array (PLA) with $N_r = N_h \times N_v$ reflective elements, where N_h and N_v denote the number of elements in the horizontal plane and the vertical direction of the absolute reference system, respectively.

We indicate by $\mathbf{b}_m \in \mathbb{R}^3$, $\mathbf{r}_n \in \mathbb{R}^3$ and $\mathbf{u} \in \mathbb{R}^3$ the locations of the m-th BS center, the n-th RIS center and the typical UE, respectively. We assume that the direct line-of-sight (LoS) links from the BSs provide negligible receive power in the target area due to blockage or severe shadowing. Therefore, the communication between BSs and UEs must be carried out over the reflected link through the RISs. In practice, we assume that each BS can leverage on multiple RISs but each RIS is used and controlled by a single BS, which connects to the on-board RIS controller via a separate (wired or wireless) reliable control link. Focusing on the downlink transmission, the m-th BS transmits data to the UE over the reflected links through the n-th RIS. Such path can be decomposed into the LoS channel $\mathbf{h}_n \in \mathbb{C}^{N_r \times 1}$ through which the RIS reflects the impinging signal towards the UE, and the LoS channel $\mathbf{G}_{mn} \in \mathbb{C}^{N_r \times N_b}$ between the BS and the RIS.

Let us indicate as Λ_m, with cardinality $|\Lambda_m|$, the set of RISs that are associated with BS m. The received downlink signal at the UE is given by the superposition of the signals incoming from all BSs through their associated RISs, namely

$$y \triangleq \sum_{m=0}^{M-1} \sum_{n=0}^{|\Lambda_m|} \left(\mathbf{h}_n^{\mathrm{H}} \boldsymbol{\Phi}_n \mathbf{G}_{mn}\right) \mathbf{w}_m s + n \in \mathbb{C}, \tag{1}$$

where $\boldsymbol{\Phi}_n = \mathrm{diag}[\alpha_{n1} e^{j\phi_{n1}}, \ldots, \alpha_{nN} e^{j\phi_{nN}}]$ with $\phi_{ni} \in [0, 2\pi]$ and $|\alpha_{ni}|^2 \leq 1$, $\forall i$ indicates the phase shifts and amplitude attenuation introduced by the n-th RIS, $\mathbf{w}_m \in \mathbb{C}^{N_b \times 1}$ is the transmit precoder at the m-th BS while $s \in \mathbb{C}$ is the transmit signal with $|s|^2 = 1$, and $n \in \mathbb{C}$ is the additive white Gaussian noise term distributed as $\mathcal{CN}(0, \sigma^2)$.

As 3rd Generation Partnership Project (3GPP) cellular standards require the UE to be served by a single BS, we remark that the UE receives useful signal only from one BS, e.g., the m-th BS, and suffers from the interference produced by all other BSs. Therefore, the received signal-to-interference-plus-noise ratio (SINR) at the UE can be written as

$$\mathrm{SINR}(\mathbf{u}) \triangleq \frac{\left| \sum_{n=0}^{|\Lambda_m|} \left(\mathbf{h}_n^{\mathrm{H}} \boldsymbol{\Phi}_n \mathbf{G}_{mn}\right) \mathbf{w}_m \right|^2}{\sum_{\substack{l=0, \\ l \neq m}}^{M-1} \left| \sum_{n=0}^{|\Lambda_l|} \left(\mathbf{h}_n^{\mathrm{H}} \boldsymbol{\Phi}_n \mathbf{G}_{ln}\right) \mathbf{w}_l \right|^2 + \sigma^2}, \tag{2}$$

where the BSs-RISs and RISs-UE channels are fully defined by knowing the geometry of the network while the RISs configurations and the BSs precoders depend on the BSs-RISs and BSs-UE associations. As shown in Fig. 3, in order to write the channels $\mathbf{h}_n$ and $\mathbf{G}_{mn}$, we first consider N reference

systems with origin in the center of each RIS and the (x', y')-plane lying on the RIS surface. Hence, the coordinates of the UE in the reference system of the n-th RIS can be obtained as $\mathbf{u}^{(n)} = \mathbf{R}_n \mathbf{u}$, where

$$\mathbf{R}_n \triangleq \begin{pmatrix} \hat{\mathbf{r}}_{n,x'} & \hat{\mathbf{r}}_{n,y'} & \hat{\mathbf{r}}_{n,z'} \end{pmatrix} \in \mathbb{R}^{3\times 3}, \tag{3}$$

with $\hat{\mathbf{r}}_{n,x'}$, $\hat{\mathbf{r}}_{n,y'}$ and $\hat{\mathbf{r}}_{n,z'} \in \mathbb{R}^3$ representing the coordinates of the n-th RIS reference system axes in the absolute reference system. Furthermore, we denote by $\psi_{\mathrm{D},n}$ and $\eta_{\mathrm{D},n}$ the azimuth and the zenith angle of departure (AoD) for the communication link from the RIS to the UE. Therefore, the RIS array response vector is given by

$$\begin{aligned} \mathbf{b}_{\mathrm{T},n}(\mathbf{u}) &\triangleq \mathbf{b}_y(\psi_{\mathrm{D},n}, \eta_{\mathrm{D},n}) \otimes \mathbf{b}_z(\psi_{\mathrm{D},n}, \eta_{\mathrm{D},n}) \in \mathbb{C}^{N_r \times 1} \qquad (4) \\ &= [1, e^{j2\pi\delta \sin(\psi_{\mathrm{D},n}) \sin(\eta_{\mathrm{D},n})}, \ldots, \\ &\quad e^{j2\pi\delta(N_y-1) \sin(\psi_{\mathrm{D},n}) \sin(\eta_{\mathrm{D},n})}]^{\mathrm{T}} \\ &\quad \otimes [1, e^{j2\pi\delta \cos(\psi_{\mathrm{D},n}) \sin(\eta_{\mathrm{D},n})}, \ldots, \\ &\quad e^{j2\pi\delta(N_x-1) \cos(\psi_{\mathrm{D},n}) \sin(\eta_{\mathrm{D},n})}]^{\mathrm{T}}, \qquad (5) \end{aligned}$$

where δ indicates the antenna spacing-wavelength ratio. We refer to $\Omega_{\mathrm{T},n}(\mathbf{u}) \triangleq \cos(\psi_{\mathrm{D},n}) \sin(\eta_{\mathrm{D},n}) = \frac{u_x^{(n)}}{\|\mathbf{u}^{(n)}\|}$ and $\Psi_{\mathrm{T},n}(\mathbf{u}) \triangleq \sin(\psi_{\mathrm{D},n}) \sin(\eta_{\mathrm{D},n}) = \frac{u_y^{(n)}}{\|\mathbf{u}^{(n)}\|}$ as the spatial frequencies along the x'_n and the y'_n-axis corresponding to the AoD towards the UE at absolute coordinates $\mathbf{u}$. Therefore, the LoS n-th RIS-UE channel is given by

$$\mathbf{h}_n(\mathbf{u}) \triangleq \sqrt{\gamma_n(\mathbf{u})}\, \mathbf{b}_{\mathrm{T}.n}(\mathbf{u}) \in \mathbb{C}^{N_r \times 1}, \tag{6}$$

where $\gamma_n(\mathbf{u}) \triangleq d_n(\mathbf{u})^{-\beta}$ is the channel power gain with $d_n(\mathbf{u}) = \|\mathbf{r}_n - \mathbf{u}\|$ being the Eucledian distance between the RIS and the UE. In a similar way, the LoS channel between the m-th BS and the n-th RIS can be written as

$$\mathbf{G}_{mn} \triangleq \sqrt{\gamma_{\mathrm{G}_{mn}}}\, \mathbf{b}_{\mathrm{R},n}(\mathbf{b}_m) \mathbf{a}_m^{\mathrm{H}}(\mathbf{r}_n) \in \mathbb{C}^{N_r \times N_b}, \tag{7}$$

where $\gamma_{\mathrm{G}_{mn}} \triangleq d_{mn}^{-\beta}$ is the channel power gain with $d_{mn} = \|\mathbf{b_m} - \mathbf{r}_n\|$, $\mathbf{a}_{\mathrm{R},n}(\mathbf{b}_m)$ is the array response vector at the RIS corresponding to the angle of arrival (AoA) from BS m, which is derived analogously to Eq. (4), and $\mathbf{a}_m(\mathbf{r}_n)$ indicates the BS array response, defined as

$$\mathbf{a}_m(\mathbf{r}_n) \triangleq [1, \ldots, e^{j2\pi\delta(M-1)\cos(\theta_{\mathrm{D},mn})}]^{\mathrm{T}} \in \mathbb{C}^{N_b \times 1}, \tag{8}$$

where $\theta_{\mathrm{D},mn}$ represents the AoD from the m-th BS to the n-th RIS.

III. Problem Formulation

Analytical tractability. The solution to our multi-RIS planning problem requires determining the optimal RISs deployment to provide coverage within the target area, e.g., by maximizing the worst-case received SINR at all locations $\mathbf{u}$. To this aim, we need to jointly optimize the active transmit beamformers at the BSs as well as the RISs placement, their passive beamforming configurations, and their controlling BSs, which in turn dictate the optimal end-to-end BS-UE associations. The resulting optimization problem is highly non-convex and extremely difficult to tackle due to the intricate coupling between the BSs-RISs and BSs-UE associations, and the joint active-passive beamforming configurations throughout the network. For instance, even for a given BS-RIS-UE association, jointly optimizing the beamforming at the BS and the RIS does not yield a closed-form formulation but rather requires tackling a non-convex problem by alternatively solving the two separate beamforming optimizations until convergence [15].

Therefore, for the sake of analytical tractability, we consider propagation paths involving only first-order RIS reflections, and assume a cellular-like architecture in which each RIS provides coverage to one contiguous subarea, thus reducing the scope of the interference generated by the remaining RISs to the sheer overlapping area edges. We would like to highlight that at planning stage, the RISs beamforming design for area coverage enhancement cannot take advantage of the knowledge of the instantaneous CSI of any particular UE in the area. Hence, although RISs controlled by the same BS can be configured to cover the same subarea, it is highly complex to enforce in-phase constructive interference of signals incoming from different RISs even if transmitted by the same BS.

Let us consider the UE to be inside the subarea served by BS m through RIS n. In these conditions, its received SINR can be then approximated by its signal-to-noise ratio (SNR), which is defined as

$$\mathrm{SNR}(\mathbf{\Phi}_n, \mathbf{w}_m, \mathbf{u}) \triangleq \frac{\left|\mathbf{h}_n^{\mathrm{H}} \mathbf{\Phi}_n \mathbf{G}_{mn}\, \mathbf{w}_m\right|^2}{\sigma^2}, \tag{9}$$

where $\mathbf{\Phi}_n$ and $\mathbf{w}_m$ need to be optimized.

Optimization variables. We assume that the RISs are deployed only at specific locations, i.e. candidate sites (CSs), to reflect the fact that network operators are required to meet logistical, administrative and physical constraints in real-life scenarios. Nonetheless, in the absence of CSs, our multi-RIS planning may be likewise executed by considering any sampling of the deployment area. For the sake of simplicity, we assume that the CSs set matches the set $\{\mathbf{r}_n\}_{n=1}^N$, namely the candidate RISs positions are pre-defined and we aim at identifying where to actually deploy RISs among them. Besides, we sample the target area by means of T test points $\mathbf{u}_t \in \mathcal{A}$, wherein we optimize the SNR of the typical UE[1]. Our planning solution outputs the set of RISs to be deployed while providing the optimal BS-RIS-UE association at each est point. We thus introduce decision variables $\mathbf{x} \in \{0,1\}^N$ and $\mathbf{y} \in \{0,1\}^{T\times M\times N}$, whose elements x_n and y_{tmn} indicate whether a RIS is deployed at CS n, and the association between the typical UE at test point $\mathbf{u}_t$, BS m and RIS at CS n, respectively.

RISs planning. We can now formulate the multi-RIS coverage enhancement problem as the following

[1]Ideally, the test point distribution should match the expected distribution of the users in the target area but the problem formulation remains valid for any distribution of users.

Problem 1 (Multi-RIS coverage enhancement):

$$\max_{\boldsymbol{\Phi}_n, \mathbf{w}_m, \mathbf{x}, \mathbf{y}} \min_{\mathbf{u}_t} \sum_{m,n} y_{tmn} \left| \mathbf{h}_n^{\mathrm{H}} \boldsymbol{\Phi}_n \mathbf{G}_{mn} \mathbf{w}_m \right|^2 \tag{10a}$$

$$\text{s.t.} \quad |\Phi_{n,ii}|^2 \leq 1, \qquad \forall n, \forall i, \tag{10b}$$

$$\|\mathbf{w}_m\|^2 \leq P, \qquad \forall m, \tag{10c}$$

$$y_{tmn}\, \hat{\mathbf{r}}_{n,x'}^{\mathrm{T}} (\mathbf{u}_t - \mathbf{r}_n) \geq 0, \qquad \forall t, \forall m, \forall n, \tag{10d}$$

$$y_{tmn}\, \hat{\mathbf{r}}_{n,x'}^{\mathrm{T}} (\mathbf{b}_m - \mathbf{r}_n) \geq 0, \qquad \forall t, \forall m, \forall n, \tag{10e}$$

$$y_{tmn} \leq x_n, \qquad \forall t, \forall m, \forall n, \tag{10f}$$

$$\sum_{m,n} y_{tmn} = 1, \qquad \forall t, \tag{10g}$$

$$\sum_{m} \max_{t} y_{tmn} \leq 1, \qquad \forall n \tag{10h}$$

$$\sum_{n} x_n = L, \tag{10i}$$

$$x_n \in [0,1], \quad y_{tmn} \in [0,1], \quad \forall t, \forall m, \forall n, \tag{10j}$$

where we omit the constant noise term σ^2 and refer to the available transmit power at the BSs as P. The constraint in Eq. (10b) ensures that the RISs are passive while the one in Eq. (10c) enforces that the BSs power budget is satisfied by each precoder $\mathbf{w}_m$. Constraints (10d) and (10e) guarantee that each RIS can respectively serve a test point or be assigned to a BS only if they front the RIS, i.e. only if the vector originated in the RIS and pointing towards the test point or the BS has a positive projection on the RIS orientation vector $\hat{\mathbf{r}}_{n,x'}$. Moreover, constraint (10f) states that a RIS should be deployed only if at least the UE located at one test point would exploit it, whereas constraint (10g) reflects the fact that each test point must be covered by only one RIS. Constraint (10h) forces each CS to be associated to at most one BS and, lastly, we enforce the number of deployed RISs to be equal to L in constraint (10i), where L is the number of RISs to be deployed by the network operator.

IV. RIS-aware Network Planning

Even disregarding the interference, Problem (1) is still highly complex due to its objective function in Eq. (10a) being the sum of non-convex elements, and the binary constraints in Eq. (10j) that make it combinatorial. Moreover, as already mentioned in Section III, the lack of knowledge about the instantaneous UEs CSI in the target area during a realistic access procedure invalidates the option of jointly configuring the RISs and BSs beamformers per UE [16]. Therefore, we decouple the RISs and BSs beamforming configurations from the planning problem itself by configuring each RIS to provide coverage to one contiguous subarea and assuming that each BS radiates all its available power towards each of its associated RISs in a time-division multiple access (TDMA) fashion. In other words, we assume that the RISs have a single-beam radiation pattern and that they do not serve more than one subareas, thereby guaranteeing that all locations belonging to one subarea are served by a single BS through one single RIS. Given sufficient coverage in the area, multiple users in each subarea can be separated by conventional multiple access techniques, such as TDMA or orthogonal frequency-division multiple access (OFDMA).

It can be easily observed from Eq. (9) that the SNR at the UE $\mathbf{u}_t$ provided by BS m through RIS n can be equivalently written as $\mathrm{SNR}(\boldsymbol{\Phi}_n, \mathbf{w}_m, \mathbf{u}_t) = \frac{g_1(\boldsymbol{\Phi}_m, \mathbf{w}_m, \mathbf{u}_t)}{g_2(\mathbf{u}_t)}$, where $g_1(\boldsymbol{\Phi}_n, \mathbf{w}_m, \mathbf{u}_t)$ provides the overall array gain due to the cascaded active and passive beamformings, while $g_2(\mathbf{u}_t)$ accounts for the concatenated BS-RIS-UE pathloss. Following [17], the RIS configuration can be obtained by means of 3D beam broadening and flattening, namely by partitioning the RIS into multiple sub-arrays of smaller size and optimizing their phase shifts to shape one single flattened beam whose beamwidth can be properly tuned to match the size of the target subarea. In particular, by denoting the subarea covered by RIS n by $\mathcal{A}_n$ and assuming $\mathbf{u}_t \in \mathcal{A}_n$, the resulting BS-RIS gain can be written as

$$g_1(\bar{\boldsymbol{\Phi}}_n, \bar{\mathbf{w}}_m, \mathbf{u}_t) \approx \frac{N_h^2}{\Delta_{n,x'} N_h \delta} \frac{N_v^2}{\Delta_{n,y'} N_v \delta}, \quad \forall \mathbf{u}_t \in \mathcal{A}_n, \tag{11}$$

where $\bar{\boldsymbol{\Phi}}_n$ is derived by means of beam broadening and flattening, and $\mathbf{w}_m$ is the maximum ratio transmission (MRT) precoder, which depends only on $\mathbf{G}_{mn}$. Besides, $\Delta_{n,x'}$ and $\Delta_{n,y'}$ respectively denote the desired spans of the spatial frequency deviations along the horizontal x'_n and vertical y'_n-axis of RIS n to cover its subarea and are defined as

$$\Delta_{n,x'} \triangleq \max_{\mathbf{u}_t \in \mathcal{A}_n} \Omega_{\mathrm{T},n}(\mathbf{u}_t) - \min_{\mathbf{u}_t \in \mathcal{A}_n} \Omega_{\mathrm{T},n}(\mathbf{u}_t), \tag{12}$$

$$\Delta_{n,y'} \triangleq \max_{\mathbf{u}_t \in \mathcal{A}_n} \Psi_{\mathrm{T},n}(\mathbf{u}_t) - \min_{\mathbf{u}_t \in \mathcal{A}_n} \Psi_{\mathrm{T},n}(\mathbf{u}_t). \tag{13}$$

The overall pathloss experienced by the UE at coordinates $\mathbf{u}_t$ is given by $g_2(\mathbf{u}_t) = d_{mn}^{\beta} d_n^{\beta}(\mathbf{u}_t)$. Therefore, we can state the following equivalent formulation for Problem (1), i.e.

Problem 2 (Multi-RIS planning):

$$\max_{\mathbf{x}, \mathbf{y}, \boldsymbol{\Delta}_{x'}, \boldsymbol{\Delta}_{y'}} \min_{\mathbf{u}_t} \sum_{m,n} y_{tmn} \frac{1}{\Delta_{n,x'} \Delta_{n,y'}} \frac{1}{d_{mn}^{\beta} d_n^{\beta}(\mathbf{u}_t)} \tag{14a}$$

$$\text{s.t.} \quad \sum_{m} y_{tmn} \left| \Omega_{\mathrm{T},n}(\mathbf{u}_t) - \Omega_{\mathrm{T},n}(\mathbf{u}_k) \right| \leq \Delta_{n,x'}, \quad \forall n, \forall \mathbf{u}_t, \mathbf{u}_k \in \mathcal{A}, \tag{14b}$$

$$\sum_{m} y_{tmn} \left| \Psi_{\mathrm{T},n}(\mathbf{u}_t) - \Psi_{\mathrm{T},n}(\mathbf{u}_k) \right| \leq \Delta_{n,y'}, \quad \forall n, \forall \mathbf{u}_t, \mathbf{u}_k \in \mathcal{A}, \tag{14c}$$

$$\Delta_{n,x'} \geq \frac{1}{N_h \delta}, \quad \Delta_{n,y'} \geq \frac{1}{N_v \delta}, \qquad \forall n, \tag{14d}$$

$$(10\text{d}), (10\text{e}), (10\text{f}), (10\text{g}), (10\text{h}), (10\text{i}), (10\text{j}),$$

in which we define $\boldsymbol{\Delta}_{x'} \triangleq [\Delta_{1,x'}, \ldots, \Delta_{N,x'}]$, $\boldsymbol{\Delta}_{y'} \triangleq [\Delta_{1,y'}, \ldots, \Delta_{N,y'}]$ while we omit the constant terms. In this equivalent formulation, we introduce the constraints in Eqs. (14b) and (14c) in order to guarantee that each test point served by RIS n lies within the coverage determined by its spatial frequency span. In Eq. (14d), we enforce that the spatial frequency spans $\boldsymbol{\Delta}_{x'}$ and $\boldsymbol{\Delta}_{y'}$ are at least as wide as the minimum beamwidth obtained by considering a single sub-array while performing the RISs configuration via beam broadening and flattening, as by [17].

V. Large-scale planning algorithm

Hereafter, we design our multi-RIS planning algorithm, i.e., RISA. Let us first consider a continuous relaxation of Problem (2) by letting $\mathbf{x} \in [0,1]^N$ and $\mathbf{y} \in [0,1]^{T\times M\times N}$ in constraint (10j). We can tackle such problem by means of BCA, namely by iteratively solving the problem for one block of optimization variables while keeping all the others fixed. Notably, although non-convex in general, the continuous relaxation of the problem is jointly convex in the block of variables $\mathbf{x}, \mathbf{y}$ while it is still non-convex neither in $\mathbf{\Delta}_{x'}$, nor in $\mathbf{\Delta}_{y'}$, as the respective objective functions are convex and their maximization leads to a non-convex problem *per se*. In order to solve the problem for $\mathbf{\Delta}_{x'}$ (or, similarly, for $\mathbf{\Delta}_{y'}$), we can rearrange Eq. (14a) as

$$\max_{\mathbf{\Delta}_{x'}} \quad \min_{\mathbf{u}_t} \sum_{m,n} \frac{y_{tmn}}{d_{mn}^2 d_n^2(\mathbf{u}_t)\Delta_{n,y'}} \frac{1}{\Delta_{n,x'}}, \tag{15}$$

and observe that the resulting subproblem belongs to the Fractional Programming (FP) umbrella, being Eq. (15) a *sum of functions of ratios*. Therefore, we can leverage on the Quadratic Transform [18] and write it equivalently as

$$\max_{\mathbf{z}_{x'},\mathbf{\Delta}_{x'}} \min_{\mathbf{u}_t} \sum_{m,n} \frac{y_{tmn}}{d_{mn}^2 d_n^2(\mathbf{u}_t)\Delta_{n,y'}} (2z_{n,x'} - z_{n,x'}^2 \Delta_{n,x'}), \tag{16}$$

where $\mathbf{z}_{x'} \in \mathbb{R}^N$ is an auxiliary optimization variable. The resulting subproblem is now convex in $\mathbf{z}_{x'}$ and in $\mathbf{\Delta}_{x'}$ separately, thus likewise solvable by means of a nested BCA.

Therefore, the solution of the continuous relaxation of Problem (2) consists of a double-nested BCA whose outer loop iteratively considers the three blocks of variables $\mathbf{x}$ and $\mathbf{y}$, $\mathbf{\Delta}_{x'}$, $\mathbf{\Delta}_{y'}$, while its inner loops solve the subproblems in $\mathbf{\Delta}_{x'}$ and $\mathbf{\Delta}_{y'}$ by introducing auxiliary variables $\mathbf{z}_{x'} \in \mathbb{R}^N$ and $\mathbf{z}_{y'} \in \mathbb{R}^N$, respectively. We would like to highlight that, by dealing with a convex problem at each stage, the double-nested BCA is guaranteed to converge to a stationary point [14].

Binary solution. The binary deployment variable $\mathbf{x}^*$ are recovered by rounding the highest L elements of $\mathbf{x}$ to 1 while setting the other $N - L$ to 0. Next, we establish the binary associations $\mathbf{y}^*$ by considering only activated CSs $\mathbf{b}_n$ such that $x_n^* = 1$. In particular, we iteratively associate each test point $\mathbf{u}_t$ by setting to 1 the highest element $\mathbf{y}$ among the ones corresponding to the activated CSs. Concurrently, we update the values of $\Delta_{n,x'}$ and $\Delta_{n,y'}$ to the minimum spatial frequency spans satisfying the constraints in Eqs. (14b), (14c).

We depict the overall high-level algorithm in Algorithm 1.

VI. Performance evaluation

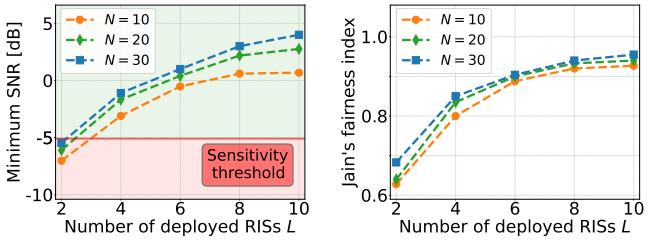
We first evaluate RISA via Monte Carlo simulations considering synthetic network topologies. Subsequently, we benchmark RISA on the real network topology installed in the *Rennes railway station*, France, provided by the European network operator *Orange*, wherein RISs Candidate Sites (CSs) are properly handpicked on the station floor plan and realistic SNR values are obtained via ray tracing. Simulation parameters based on realistic values are listed in Table I, unless otherwise stated.

Algorithm 1: RIS-Aware network planning (RISA)

Initialize $\Delta_{n,x'} = \Delta_{n,y'} = 2$, $n = 1, \ldots, N$
repeat *Outer BCA loop*
  Solve the continuous relaxation of Problem 2 jointly for $\mathbf{x}$ and $\mathbf{y}$
  repeat *First inner BCA loop*
    Solve the transformed problem in $\mathbf{\Delta}_{x'}$ for $\mathbf{z}_{x'}$
    Solve the transformed problem in $\mathbf{\Delta}_{x'}$ for $\mathbf{\Delta}_{x'}$
  until *convergence of objective function in Eq.* (15)
  repeat *Second inner BCA loop*
    Solve the transformed problem in $\mathbf{\Delta}_{y'}$ for $\mathbf{z}_{y'}$
    Solve the transformed problem in $\mathbf{\Delta}_{y'}$ for $\mathbf{\Delta}_{y'}$
  until *convergence of objective function in Eq.* (15) *for* $\Delta_{y'}$
until *convergence of objective function Eq.* (14a) *in Problem 2*
Round $\mathbf{x}$ and $\mathbf{y}$ to derive binary $\mathbf{x}^*$ and $\mathbf{y}^*$ as by Section V

TABLE I: Simulation parameters.

Parameter	Value	Parameter	Value	Parameter	Value
P	28 dBm	f	26 GHz	σ^2	-80 dBm
β	2	μ	0.5	A	100 m × 100 m
BSs (M)	2	CSs (N)	{10,20,30}	T	100
N_b	2	N_r	350 × 175	N_{ref}	2



(a) RISA SNR performance. (b) RISA fairness performance.

Fig. 4: RISA performance with different numbers of deployed RISs and available Candidate Sites (CSs) via Monte Carlo simulations considering synthetic topologies.

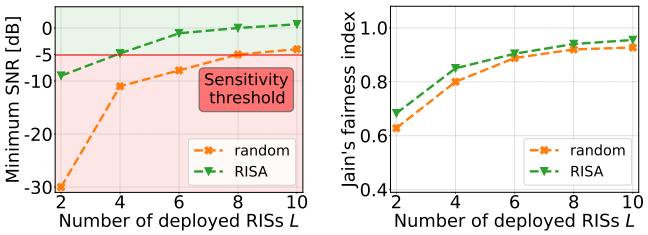
Synthetic topologies. We consider the target area to be a square surface with area $A = 100\,\text{m} \times 100\,\text{m}$. Besides, we assume that $M = 2$ BSs are placed at the bottom-left and upper-right corners of the area, namely $\mathbf{b}_1 = [0, 0, 5.5]^{\mathrm{T}}$, $\mathbf{b}_2 = [10^3, 10^3, 5.5]^{\mathrm{T}}$, while we evaluate the SNR performance at $T = 100$ test points uniformly distributed in the target area on the plane $z = 1.5$. We average the results over 10^3 Monte Carlo executions. In Fig. 4(a), we show the performance of RISA in terms of minimum SNR experienced in the target area with respect to the number of deployed RISs L for different numbers of available CSs $N = \{10, 20, 30\}$ on the plane $z = 5.5$. The horizontal line indicates the minimum SNR threshold to meet the receiver sensitivity. As expected, the minimum SNR shows a positive monotonic behavior with decreasing relative increments, thus suggesting the existence of an optimal value for L, e.g. $L = 8$ deployed RISs for $N = 10$ candidate sites. Besides, increasing the number of

CSs does not significantly benefit the overall performance, provided that the number of CSs is big enough to obtain a good sampling of the target area (on average). The SNR fairness among test points, measured by means of the Jain's fairness index (JFI) [19], shows a similar behavior[2] in Fig. 4(b), validating our *max-min* objective function design choice to enhance coverage in the whole area.

Rennes station. We execute the ray-tracing simulation in MATLAB R2021b using a simplified 3D model of the main floor of the Rennes railway station in France. The scenario follows the most prominent obstacles and elements filling the volume object of study. Highly convoluted or unknown elements (e.g., the ceiling, composed of many structural, functional, and decorative beams, as well as the tubing, etc.) have been left as holes to simulate the lack of significant, predictable reflections and lessen the computational burden. The resulting model has 579 triangles, 1582 edges and 1053 vertexes and is depicted in Fig. 1. We simulate the BSs with $N_b = 2$ and transmit power $P = 28$ dBm at $f = 26$ GHz, as in the real network deployment by *Orange*. Besides, we implement shooting and bouncing rays (SBR) in order to derive the possible paths to reach any given test point [20]. We linearly combine the power received at any test point from different paths assuming a (uniformly distributed) random phase for each individual path at the UE side, thereby accounting for random external factors (e.g., thermal expansion) that could alter the path lengths by a non-negligible fraction of a wavelength $\lambda = 1/f$, given the large ratio between the station distances and the wavelength [21]. The maximum number of reflections is set to $N_{ref} = 2$ as higher-order reflections provide little contribution to the received power.

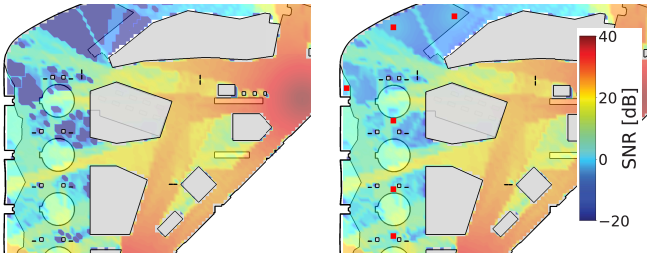
RIS ray-tracing model. We would like to underline that RISs are novel network devices, thereby not yet widely implemented in conventional ray-tracers. Therefore, we devise a new lightweight technique to compute the impinging power on the RIS surface, the RIS power reflection and the RIS beampattern. To estimate the impinging power on the RIS surface, we assess the power received at the RIS center by one of its elements modeled as a cosine antenna (with exponent parameter $\mu = 0.5$) and multiply this value by the number of RIS elements N_r. Hence, we simulate the RIS controlled reflections by considering outgoing rays originated on the RIS surface with power equal to the RIS impinging power. The RIS emissive beampattern is modeled as a uniform rectangular array (URA) of N_r cosine antennas, where the phase shifts of each element is controlled with narrow-band phase-shift beamforming. Lastly, we compute the received power at each test point by adding up the power from each source of any incident ray as received by an isotropic antenna placed at the test point coordinates. Note that we assume a power-based association policy, namely we consider each test point to be associated to the BS providing the highest power, either over the direct link or via reflections through the deployed RISs.

[2]Note that, to obtain meaningful numerical results for the JFI, we prevent the received power from exceeding a given maximum, i.e. -65 dBm, which provides excellent Receive Signal Strength Indicator (RSSI).



(a) RISA SNR performance. (b) RISA fairness performance.

Fig. 5: RISA performance obtained via ray-tracing simulations for different numbers of deployed RISs and available Candidate Sites (CSs) in a realistic environment (Rennes station).



(a) SNR heatmap with $L = 0$ (b) SNR heatmap with $L = 6$ RISs (red squares).

Fig. 6: SNR heatmap in the dead zone (see Figure 1) of the Rennes station obtained via ray-tracing simulations.

Realistic simulations. In Fig. 5, we show the performance of RISA for different numbers of deployed RISs among $N = 20$ handpicked CSs at a height of 5.5 m and meeting the architectural constraints of the station building. Besides, we compare such results with a random deployment policy averaged over 10^2 instances. Clearly, RISA outperforms the random policy in both metrics, i.e., minimum SNR in Fig. 5(a) and JFI in Fig. 5(b). The fairness is further confirmed in Fig. 6, wherein we compare the 2D heatmaps of the SNR obtained by RISA for $L = 6$ numbers of deployed RISs against the baseline with no RIS.

VII. Conclusions

RISs introduce a novel challenge in traditional cellular networks planning. On the one hand, optimal RISs configurations should be computed given fixed BSs and RISs positions. On the other hand, optimal RISs deployments depend on RISs configurations. To address these coupled issues and make the analysis tractable, in this paper we proposed RISA, a RIS-aware network planning solution that builds on double-nested block coordinate ascent to provide an iterative solution to this unprecedented problem. RISA is evaluated on synthetic generic indoor network deployments and in a real railway station (Rennes). Our results show that RISA can i) achieve outstanding performance on top of the existing network infrastructure, ii) solve the dead-zone problem in highly-crowded environments and iii) improve the user fairness at very limited installation costs.

REFERENCES

[1] E. Björnson, O. Özdogan, and E. G. Larsson, "Reconfigurable Intelligent Surfaces: Three Myths and Two Critical Questions," *IEEE Communications Magazine*, vol. 58, no. 12, pp. 90–96, 2020.

[2] E. C. Strinati, G. C. Alexandropoulos, H. Wymeersch, B. Denis, V. Sciancalepore, R. D'Errico, A. Clemente, D.-T. Phan-Huy, E. De Carvalho, and P. Popovski, "Reconfigurable, Intelligent, and Sustainable Wireless Environments for 6G Smart Connectivity," *IEEE Communications Magazine*, vol. 59, no. 10, pp. 99–105, 2021.

[3] E. C. Strinati, G. C. Alexandropoulos, V. Sciancalepore, M. Di Renzo, H. Wymeersch, D.-T. Phan-Huy, M. Crozzoli, R. D'Errico, E. De Carvalho, P. Popovski, P. Di Lorenzo, L. Bastianelli, M. Belouar, J. E. Mascolo, G. Gradoni, S. Phang, G. Lerosey, and B. Denis, "Wireless Environment as a Service Enabled by Reconfigurable Intelligent Surfaces: The RISE-6G Perspective," in *2021 Joint European Conference on Networks and Communications 6G Summit (EuCNC/6G Summit)*, 2021, pp. 562–567.

[4] A. Albanese, V. Sciancalepore, and X. Costa-Pérez, "First Responders Got Wings: UAVs to the Rescue of Localization Operations in Beyond 5G Systems," *IEEE Communications Magazine*, vol. 59, no. 11, pp. 28–34, 2021.

[5] M. Di Renzo, A. Zappone, M. Debbah, M.-S. Alouini, C. Yuen, J. de Rosny, and S. Tretyakov, "Smart Radio Environments Empowered by Reconfigurable Intelligent Surfaces: How It Works, State of Research, and The Road Ahead," *IEEE Journal on Selected Areas in Communications*, vol. 38, no. 11, pp. 2450–2525, 2020.

[6] A. Albanese, F. Devoti, V. Sciancalepore, M. Di Renzo, and X. Costa-Pérez, "MARISA: A Self-configuring Metasurfaces Absorption and Reflection Solution Towards 6G," in *IEEE INFOCOM 2022 - IEEE Conference on Computer Communications*, 2022.

[7] M. Di Renzo, M. Debbah, D.-T. Phan-Huy, A. Zappone, M.-S. Alouini, C. Yuen, V. Sciancalepore, G. C. Alexandropoulos, J. Hoydis, H. Gacanin *et al.*, "Smart radio environments empowered by reconfigurable AI meta-surfaces: an idea whose time has come," *EURASIP Journal on Wireless Communications and Networking*, vol. 2019, no. 1, pp. 1–20, May 2019.

[8] A. Pitilakis, O. Tsilipakos, F. Liu, K. M. Kossifos, A. C. Tasolamprou, D.-H. Kwon, M. S. Mirmoosa, D. Manessis, N. V. Kantartzis, C. Liaskos, M. A. Antoniades, J. Georgiou, C. M. Soukoulis, M. Kafesaki, and S. A. Tretyakov, "A Multi-Functional Reconfigurable Metasurface: Electromagnetic Design Accounting for Fabrication Aspects," *IEEE Transactions on Antennas and Propagation*, vol. 69, no. 3, pp. 1440–1454, 2021.

[9] J. G. Andrews, F. Baccelli, and R. K. Ganti, "A Tractable Approach to Coverage and Rate in Cellular Networks," *IEEE Transactions on Communications*, vol. 59, no. 11, pp. 3122–3134, 2011.

[10] E. Amaldi, A. Capone, and F. Malucelli, "Planning UMTS base station location: optimization models with power control and algorithms," *IEEE Transactions on Wireless Communications*, vol. 2, no. 5, pp. 939–952, 2003.

[11] A. Fascista, A. Coluccia, H. Wymeersch, and G. Seco-Granados, "Millimeter-Wave Downlink Positioning With a Single-Antenna Receiver," *IEEE Transactions on Wireless Communications*, vol. 18, no. 9, pp. 4479–4490, 2019.

[12] A. Albanese, P. Mursia, V. Sciancalepore, and X. Costa-Pérez, "PAPIR: Practical RIS-aided Localization via Statistical User Information," in *2021 IEEE 22nd International Workshop on Signal Processing Advances in Wireless Communications (SPAWC)*, 2021, pp. 531–535.

[13] E. Moro *et al.*, "Planning Mm-Wave Access Networks With Reconfigurable Intelligent Surfaces," in *2021 IEEE 32nd Annual International Symposium on Personal, Indoor and Mobile Radio Communications (PIMRC)*, 2021, pp. 1401–1407.

[14] L. Grippo *et al.*, "On the Convergence of the Block Nonlinear Gauss-Seidel Method under Convex Constraints," *Oper. Res. Lett.*, vol. 26, no. 3, p. 127–136, Apr. 2000.

[15] Q. Wu and R. Zhang, "Intelligent Reflecting Surface Enhanced Wireless Network via Joint Active and Passive Beamforming," *IEEE Transactions on Wireless Communications*, vol. 18, no. 11, pp. 5394–5409, 2019.

[16] P. Mursia, V. Sciancalepore, A. Garcia-Saavedra, L. Cottatellucci, X. C. Pérez, and D. Gesbert, "RISMA: Reconfigurable Intelligent Surfaces Enabling Beamforming for IoT Massive Access," *IEEE Journal on Selected Areas in Communications*, vol. 39, no. 4, pp. 1072–1085, 2021.

[17] H. Lu, Y. Zeng, S. Jin, and R. Zhang, "Aerial Intelligent Reflecting Surface: Joint Placement and Passive Beamforming Design With 3D Beam Flattening," *IEEE Transactions on Wireless Communications*, vol. 20, no. 7, pp. 4128–4143, 2021.

[18] K. Shen and W. Yu, "Fractional Programming for Communication Systems—Part I: Power Control and Beamforming," *IEEE Transactions on Signal Processing*, vol. 66, no. 10, pp. 2616–2630, 2018.

[19] A. B. Sediq, R. H. Gohary, R. Schoenen, and H. Yanikomeroglu, "Optimal Tradeoff Between Sum-Rate Efficiency and Jain's Fairness Index in Resource Allocation," *IEEE Transactions on Wireless Communications*, vol. 12, no. 7, pp. 3496–3509, 2013.

[20] R. Brem and T. F. Eibert, "A Shooting and Bouncing Ray (SBR) Modeling Framework Involving Dielectrics and Perfect Conductors," *IEEE Transactions on Antennas and Propagation*, vol. 63, no. 8, pp. 3599–3609, 2015.

[21] T. S. Rappaport, *Wireless Communications: Principles and Practice, Second edition*. Prentice Hall, 2001.